horticulturae

MDPI

Article

Physiological Disorder Diagnosis of Plant Leaves Based on Full-Spectrum Hyperspectral Images with Convolutional Neural Network

Myongkyoon Yang

Smart Agriculture Innovation Center, Kyungpook National University, Daegu 41566, Korea; yangmk@knu.ac.kr

Abstract: The prediction and early detection of physiological disorders based on the nutritional conditions and stress of plants are extremely vital for the growth and production of crops. High-throughput phenotyping is an effective nondestructive method to understand this, and numerous studies are being conducted with the development of convergence technology. This study analyzes physiological disorders in plant leaves using hyperspectral images and deep learning algorithms. Data on seven classes for various physiological disorders, including normal, prediction, and the appearance of symptom, were obtained for strawberries subjected to artificial treatment. The acquired hyperspectral images were used as input for a convolutional neural network algorithm without spectroscopic preprocessing. To determine the optimal model, several hyperparameter tuning and optimizer selection processes were performed. The Adam optimizer exhibited the best performance with an F1 score of $\geq$0.95. Moreover, the RMSProp optimizer exhibited slightly similar performance, confirming the potential for performance improvement. Thus, the novel possibility of utilizing hyperspectral images and deep learning algorithms for nondestructive and accurate analysis of the physiological disorders of plants was shown.

Keywords: convolutional neural network; hyperspectral image; optimizer; phenotyping; physiological disorder; early diagnosis

check for updates

Citation: Yang, M. Physiological Disorder Diagnosis of Plant Leaves Based on Full-Spectrum Hyperspectral Images with Convolutional Neural Network. *Horticulturae* **2022**, *8*, 854. https://doi.org/10.3390/horticulturae8090854

Academic Editors: Yushan Qiao, Zhihong Zhang and Jiyu Zhang

Received: 30 August 2022
Accepted: 16 September 2022
Published: 19 September 2022

Publisher's Note: MDPI stays neutral with regard to jurisdictional claims in published maps and institutional affiliations.

Copyright: © 2022 by the author. Licensee MDPI, Basel, Switzerland. This article is an open access article distributed under the terms and conditions of the Creative Commons Attribution (CC BY) license (https://creativecommons.org/licenses/by/4.0/).

1. Introduction

Plant phenotyping can be used to diagnose physiological disorders in plants. Physiological disorders related to plant stress or nutritional conditions significantly impact the growth with irreversible changes in size and development and a change in form and function [1]. These biotic and abiotic factors reduce productivity. Furthermore, since these stimuli cause external changes, such as changes in color, shape, and the temperature of leaves, and internal changes that affect various mechanisms, identifying symptoms in advance, conducting observations before they occur, and early detection of symptoms are essential [2].

Methods for identifying the symptoms of physiological disorders in plants can be divided into two types: destructive and nondestructive methods. Although destructive methods are mostly accurate, they are time consuming and the sample cannot be reused. With the development of technology, various studies have utilized nondestructive methods. Particularly, the application of image data, which is a representative nondestructive method, is an analysis method that can be used in not only the laboratory but also remote sensing [3]. Among the various image data, hyperspectral images utilize the visible/near infrared spectrum information for analysis, which is difficult to understand with general RGB images; thus, various studies are utilizing hyperspectral images [4]. The spectrum method is a fast and simple analysis method that enables the analysis of quality and quantity using the entire spectrum or multiple wavelengths. Additionally, it is widely used in agriculture because of its speed, efficiency, reproducibility, and convenience.

Hyperspectral images have been extensively studied via traditional spectroscopic analysis methods. Pandey et al. [5] confirmed the usefulness of hyperspectral imaging to quantify the in vivo chemical properties of corn and soybeans. They acquired images for stressed leaves and developed a partial least squares regression (PLSR) model to determine its usefulness, but they determined that testing was required for various species and stages. Hyperspectral imaging was also used to evaluate rice growth and nitrogen status in a nondestructive way [6]. Furthermore, they used the PLSR model and claimed to have satisfied the precision and accuracy required through the calibration and validation process. Elvanidi et al. [7] argued the importance of the early detection of water deficit stress. Changes in tomato crops for four different irrigation treatments were analyzed using several statistical methods. Existing spectroscopic analysis methods were used to predict not only the condition of crops but also various factors such as insect damage and nutrient deficiency [8–11].

With the application of several convergence technologies and advanced algorithms in agriculture, spectral imaging is becoming an essential element in smart agriculture [12]. Furthermore, application to most agricultural industries such as monitoring, job control, and UAV utilization is being attempted, and research is being conducted to predict various phenomena [13]. Especially, with the development of computing power, various machine learning algorithms beyond traditional spectroscopic analysis are being applied. Rumpf et al. [14] employed hyperspectral image data analysis using a vegetation index and support vector machine algorithm for the early detection of diseases in sugar beet. They obtained detection performance of 65–90%, showing the validity of the analysis. Additionally, they combined the existing spectroscopic analysis method and machine learning algorithm to detect diseases in glycyrrhiza seeds [15]. Various studies have also analyzed the application of machine learning algorithms to hyperspectral images to replace or supplement existing algorithms [16–18].

The most popular artificial intelligence algorithm in recent years is deep learning. It improves performance by including a feature extraction process to obtain information from the data in the algorithm and is in large part responsible for the increased demand for artificial intelligence in various agricultural fields [19]. The application of deep learning algorithms to hyperspectral images has a strong aspect of trial, and convolutional neural networks (CNNs), a deep learning method related to image processing, are being applied [20]. Han et al. [21] developed a classifier based on peroxide values by combining hyperspectral imaging and deep learning to evaluate nut quality. Their detection performance was 93.48% for 2300 subimages, and they also analyzed the performance evaluation of the classifier. One study employed deep learning to determine the degree of cold damage of corn seedlings [22]. They employed preprocessing for hyperspectral images to simplify the calculations and obtained a correlation of 0.8219 with the results of the chemical method, proving the application potential.

In order to apply a new kind of data to the CNN algorithm, it is necessary to consider various hyperparameters. Among several hyperparameters, the optimizer is the factor that determines stability and speed in the training process. CNN is utilized for various recognition of crops, especially in agriculture, and studies that attempt optimizer analysis are being conducted. Transfer learning was used for identification and selection of ripe fruits, and analysis was performed using several hyperparameters including an optimizer [23]. In addition, a study was also conducted to find the optimal conditions through comparison of six optimizers using public data on plant diseases [24]. Most of the research utilizes RGB images, and various analyses on plant diseases and optimizers have been performed [25–27].

Compared to the application of deep learning to RGB and spectral images in agriculture [28,29], the application of hyperspectral images exhibits some differences. Since hyperspectral images contain more data than other images, they have large sizes and are difficult to analyze. Thus, they are often used in a passive or limited way when applying a new algorithm [30–32]. Accordingly, most studies employ hyperspectral images for simple

classifications or employ multispectral images rather than hyperspectral images. Since algorithms for hyperspectral image analysis are limited, various specific applications need to be analyzed.

This study analyzes physiological disorders in plant leaves by applying a deep learning algorithm to hyperspectral data. Hyperspectral images of leaves were obtained for strawberry seedlings artificially subjected to nutritional deficiency, a physiological disorder. A deep learning algorithm was used to predict and diagnose nutritional deficiencies in the images, and the effect on the optimizer was particularly closely examined. Notably, the unique distinguishing features of this study are as follows: (1) hyperspectral images applied to deep learning herein were not subjected to spectroscopic preprocessing. Existing studies mainly used data wherein the number of wavelengths was limited and thus applied various preprocessing methods to images. Although preprocessing methods are useful for removing unnecessary data, they could remove useful data during the application of a new algorithm; (2) an appropriate deep learning model was presented for full-spectrum hyperspectral images. Since the data of the deep learning algorithm used in agriculture mainly comprise RGB images, utilizing existing models is difficult. Therefore, an appropriate model was developed and selected for the data to be used; and (3) as it is a novel method, analysis was performed to select the hyperparameters of the deep learning algorithm suitable for the full-spectrum hyperspectral data. Comparison was performed focusing on the optimizer, among the various hyperparameters.

2. Materials and Methods

2.1. Hyperspectral Imaging System

2.1.1. 3D Crop Extraction

Hyperspectral images were used to identify nutritional deficiencies, which are physiological disorders in plants. A hyperspectral imaging system that is suitable for plants was custom made (Figure 1). Using the system, top and side view images can be obtained according to the growth status of crops, and the wavelength band of the camera was configured in the 400–1000 nm band, which is often used for phenotyping [33]. Hyperspectral images were obtained using a line scan method called the push-broom method. The system comprises a hyperspectral imaging camera (Pika L, Resonon Inc., Bozeman, MT, USA), a camera lens (Schneider Xenoplan 1.4/17 mm, Bad Kreuznach, Germany), a stepper motor for vertical and horizontal scanning, and four 12 V/45 W tungsten halogen illuminators. Image data were acquired using the Spectronon Pro (Resonon Inc., Bozeman, MT, USA) program.

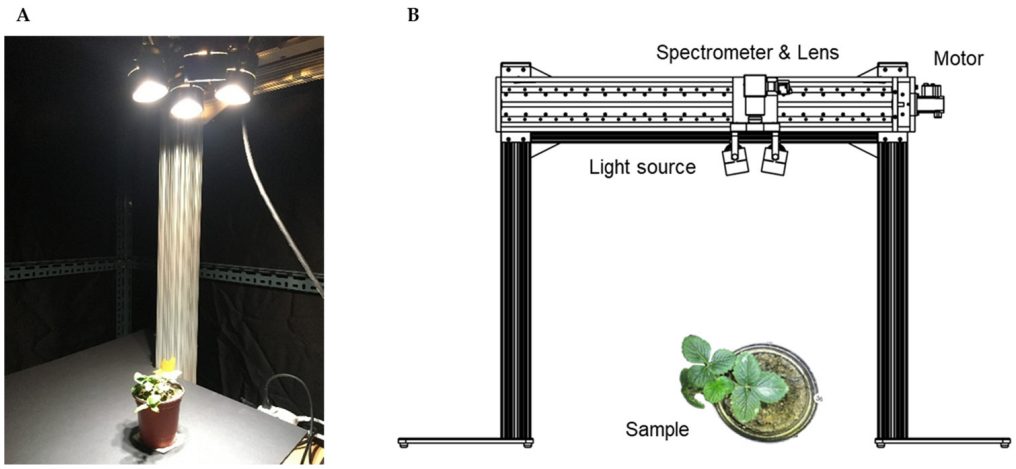

Figure 1. Hyperspectral imaging system designed for crop phenotyping: (**A**) hyperspectral image lab dark room environment and (**B**) system overview.

The wavelength band that could be actually acquired through the system was 392.91–1034.01 nm, and the wavelength resolution was 2.14 nm, which enabled detailed analysis. However, the generation of considerable noise at both ends of the measurable wavelength band due to the influence of the sensor itself needs to be considered. Since the spatial resolution of the image acquired through the device in this experimental environment was 600 × 900 pixels, each hyperspectral image was in the form of a data cube called a hypercube with 600 × 900 × 300 pixels, including 300 wavelength bands. For the hyperspectral images, scattering due to various light conditions is a problem; thus, a non-reflective black cover was installed throughout the imaging system space for stabilization. In this darkroom, only the lighting provided by the imaging system was affected.

2.1.2. Hyperspectral Image Calibration

Image acquisition through the hyperspectral system required an additional calibration process. The calibration was divided into light stabilization, black and white balance, and focus and aspect ratio. First, light stabilization was performed while operating the hyperspectral system: the bulb was opened for 10 min to stabilize the emitted radiation. Next, the black and white balance process was performed to utilize the corrected relative reflectance by measuring two types of reference values. Two types of reference images were measured through the dark calibration, which was performed by blocking the camera lens, and a standard Teflon plate that reflects about 99% of incident light was used for the white calibration. As shown in Equation (1), the relative reflectance was calculated using these two reference images and applied [34].

$$R_c = \frac{I_r - I_d}{I_w - I_d} \quad (1)$$

where R_c is the calibrated reflectance image, I_r is the raw image, I_d is the dark reference image, and I_w is the white reference image.

2.2. Data Acquisition and Plant Physiological Disorder Samples

2.2.1. Target Crops and Physiological Disorders

For the experiment, 36 seedlings of strawberry (*Fragaria* × *ananassa*) "Seolhyang" were used. In order to maintain independence, each seedling was grown in a soil cultivation environment using individual pots rather than a hydroponic environment sharing a root part, and the experiment was performed for about 60 days. The seedlings were divided into 4 groups, and the amount of water given each day was varied. The groups were divided based on the normal amount of water supplied to crops according to the seedling growth and the amount of soil: 0, 0.5, 1, and 1.5 times. No nutrients other than water were given, and consequently, the plants exhibited physiological disorders due to nutritional deficiency; hyperspectral image data of the leaves were obtained. The degree of physiological disorder was not related to the amount of water supplied; the amount of water was varied simply to afford various conditions and obtain varying responses.

A plant cultivation system was used to ensure that all conditions other than the amount of water were the same. In this system, temperature (10–30 °C), humidity (20–90%), illuminance (0–20,000 lux), and light source color were adjustable. The experiment was conducted at temperature of 20 °C, humidity of 60%, and illumination of 8000 lux (07:00–19:00). Furthermore, environmental control was not a direct part of the physiological disorder phenomenon, like the amount of water. However, the purpose was to avoid problems caused by diseases and insects other than moisture and nutritional deficiencies. Subsequently, several physiological disorder phenomena were confirmed (Figure 2).

The physiological disorders in the leaves of strawberry seedlings were classified into seven categories. Nitrogen (N) is essential for stem and leaf growth and fruit development. In case of deficiency, the color of mature leaves becomes pale and changes to yellow and red without changes in size [35]. For boron (B) deficiency, the leaves were grouped together with N because it displayed yellowing in the early stage. Accordingly, three classifications

were made: early prediction, early yellowing, and late. In case of potassium (K) deficiency, browning occurs at the edge of the leaf and gradually progresses inward. Lastly, in the case of magnesium (Mg) deficiency, it appears around the leaf and gradually burns to the leaf veins. The leaf overall appears bright yellowish-white and displays necrosis [36]. Potassium and magnesium deficiencies were grouped and divided into two categories: early prediction and symptomatic. Accordingly, classification analysis was performed for seven categories: normal, wilt, N and B deficiencies with 3 classes, and K and Mg with 2 classes.

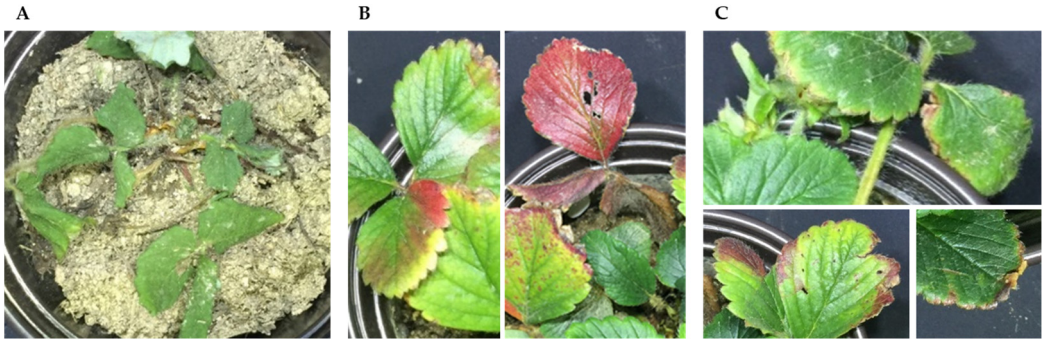

Figure 2. Symptoms of physiological disorders in experimental plants: (**A**) wilt, (**B**) yellowing of leaves, and (**C**) browning of leaves.

2.2.2. Data Preprocessing

Figure 3 shows the overall workflow of this study. Strawberry seedlings with various physiological disorders were photographed through the hyperspectral imaging system. Here, the hyperspectral camera was calibrated before shooting, as discussed above. For the acquired hyperspectral images, a process was performed to obtain information on the desired part, and the data were divided in a manner applicable to the training algorithm. Thus, a model was established, and the final performance evaluation was performed. MATLAB R2019a (The MathWorks Inc., Natick, MA, USA), Spectronon Pro, and Python 3.6 were used for the processing.

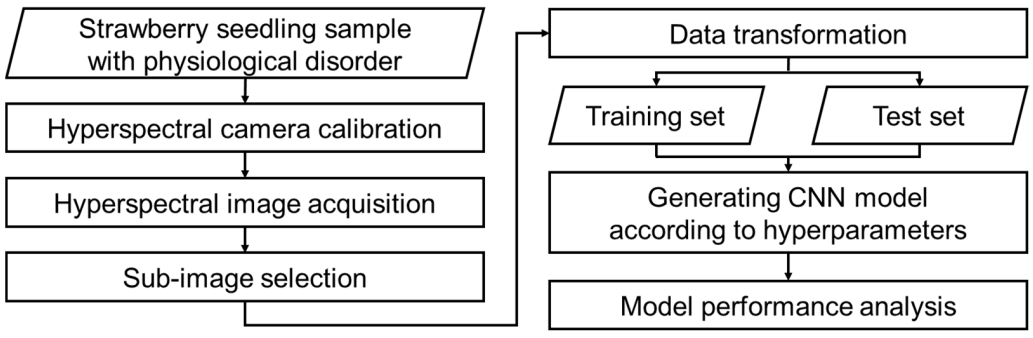

Figure 3. Overall workflow for data processing and analysis.

In each acquired hyperspectral image, various growth data were mixed. The entire seedling could be healthy, but a leaf might exhibit a single physiological disorder. In some cases, several phenomena were simultaneously observed on a leaf. Accordingly, a sub-image selection process was required according to the class group condition to be diagnosed in an image. Figure 4 provides an example of this process. A small area was designated for the part of the leaf exhibiting specific symptoms, and the images were separately saved. Predictive data were obtained by checking the healthy leaf image of the previous time for the same point based on the symptom onset time. Each sub-image had the form of a data cube with $16 \times 16 \times 300$ pixels.

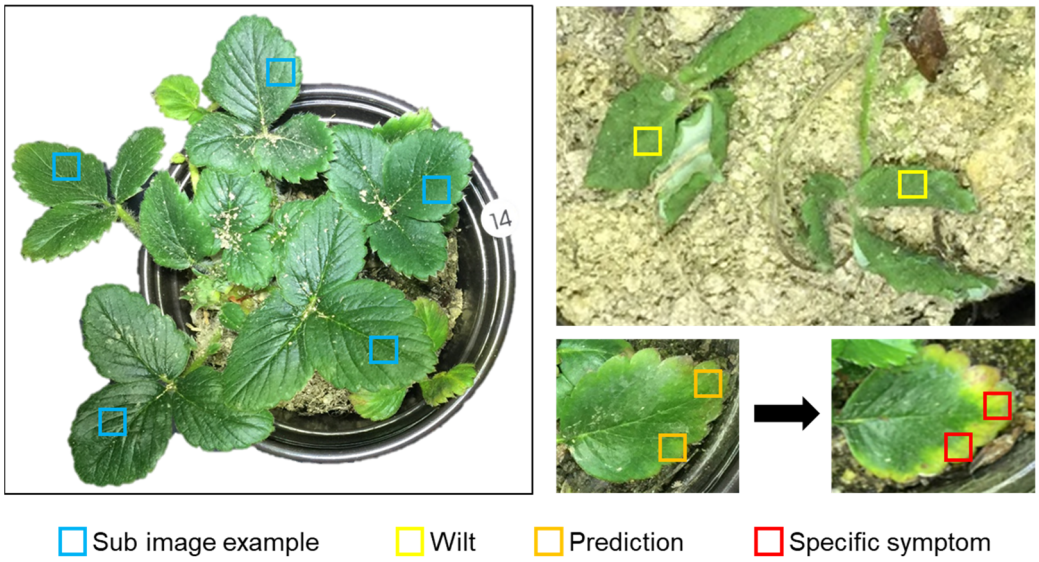

Figure 4. Example of obtaining subimages corresponding to each class from hyperspectral images of leaves.

A relatively large amount of training data is required for deep learning analysis, which is the algorithm employed herein. Accordingly, a large number of subimages were acquired, and the number of data acquired for the seven classes is shown in Table 1. A class number was assigned to each physiological disorder class, and the data were randomly divided and used with a ratio of 9:1 for training and testing. To avoid overfitting problems and consider variance, the training data were randomly mixed while creating the model and then divided into training and validation data. Subsequently, the total data were divided with a ratio of 7:2:1 for training, validation, and testing.

Table 1. Number of samples in the training, validation, and test categories for physiological disorders.

Symptom	Class Abbr.	Training	Validation	Test	Total
Normal	Nor	404	120	60	584
Wilt	Wilt	390	104	58	552
N, B deficiency prediction	NBpr	329	98	45	472
N, B deficiency Stage 1	NBd1	438	121	65	624
N, B deficiency Stage 2	NBd2	289	73	38	400
K, Mg deficiency prediction	KMpr	311	85	52	448
K, Mg deficiency	KMd	453	133	54	640
Total		2614	734	372	3720

2.3. Deep Learning-Based Diagnosis Technology

2.3.1. Diagnosis Model

Several traditional preprocessing methods exist for hyperspectral image analysis. Normalization and Savitzky–Golay filtering methods are used to minimize the spectrum noise generated from sensors, and multiplicative scattering correction and standard normal variate methods are employed for scattering correction. Additionally, since the number of channels corresponding to a wavelength is very large, the wavelength selection algorithm has been employed to remove the correlation between channels. However, the method employed herein utilizes raw subimages without performing traditional preprocessing methods. Data simplification with existing methods reduces the amount of calculations by only using data that are advantageous for analysis; however, considerable data can be discarded in this process [37]. Thus, a method utilizing the entire image without discarding information was employed herein.

Deep learning, an algorithm applied with neural networks, differs from existing machine learning algorithms; it includes feature extraction in the algorithm and exhibits good performance. Among the various deep learning methods, CNN has been widely applied in problems related to image analysis and in various studies related to plants [38].

CNN mimics human visual neurons, particularly their activation by stimuli only in the receptive field, a limited area of the field of view. Local information about the entire data is acquired using a small filter or kernel for the input data. Advantageously, the same filter can be used to obtain the local information required for image analysis while reducing the number of parameters. In contrast to the fact that the existing algorithms for analyzing hyperspectral images require several preprocessing methods, CNN can beneficially perform analysis using relatively few preprocessing algorithms. Figure 5 shows the CNN structure. The hyperspectral imaging data to be used as input and the CNN model comprising three types of layers can be confirmed. To remove the influence of the changes in the position and size of the object in the input image, a convolution operation that extracts features using a filter and a pooling operation that is a compression process were performed. These two types of operations were performed several times, and finally, the output emerges through the layer corresponding to the classification [39].

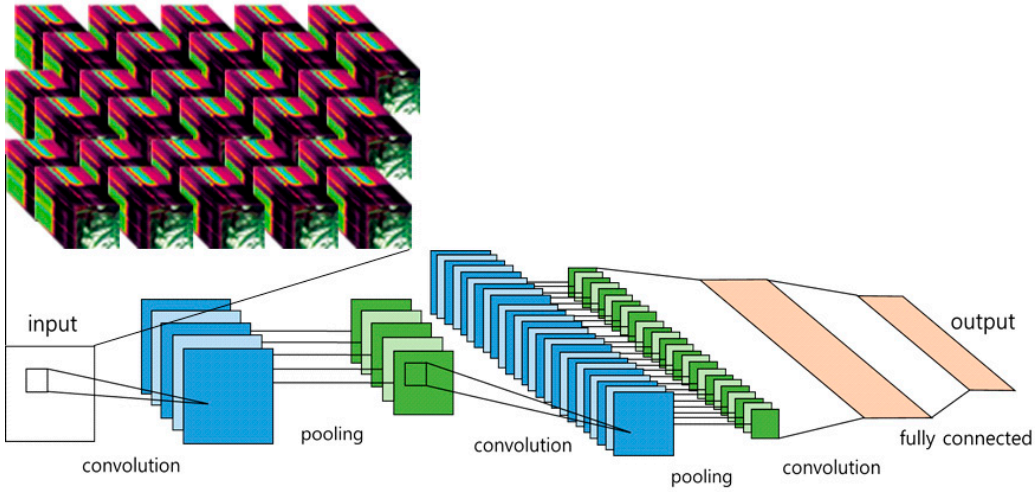

Figure 5. Hyperspectral data and CNN model structure.

2.3.2. CNN Architecture

Figure 6 shows the model architecture used herein. To examine the effect of the optimizer on the diagnosis of physiological disorders in the full-spectrum hyperspectral image, the other hyperparameters of the CNN were kept the same. Four convolutional and pooling layers of the model were employed, and two fully connected layers were used as a classifier. Generally, the convolutional and pooling layers were alternately positioned; thus, they were similarly arranged. The convolution layer, where the input data first enters, had the same channels as the hyperspectral image size, and the number of channels decreased with increasing layer depth. A small kernel size of the convolution process was employed as it is advantageous, and max pooling was used for pooling. Since the fully connected layer had a general neural network structure, it required an extremely large number of parameters compared to the other layers. Many parameters increase the likelihood of overfitting. Thus, dropout was applied between the layers to avoid overfitting and to afford a robust model in terms of speed. ReLU was used for the overall activation function, and the Softmax function was used only for the last classifier. Normalized data were used as inputs to ensure fast training and a certain range of values. Additionally, in the training process, an appropriate batch size was set to increase the efficiency, and an early stopping condition was added to prevent unnecessary training execution.

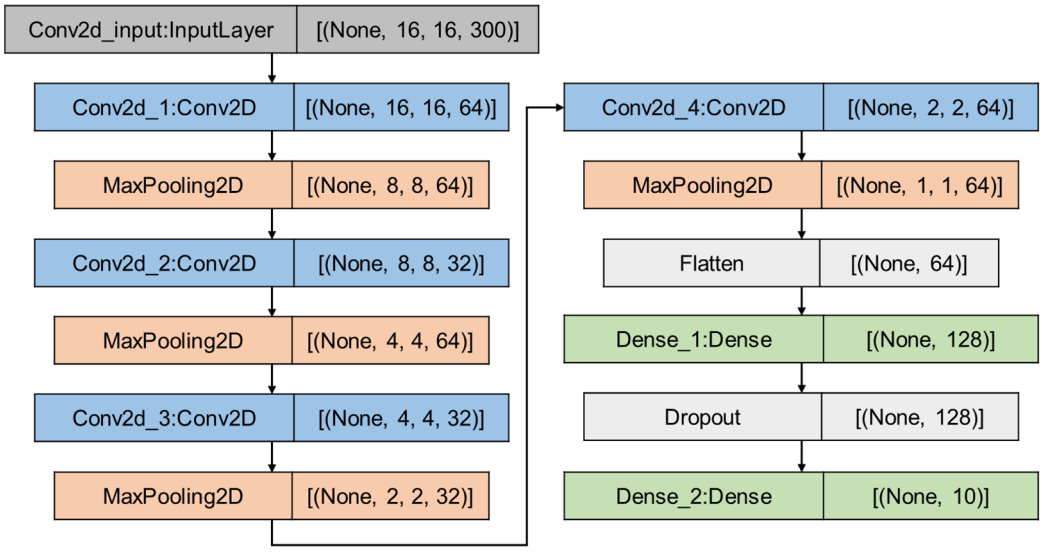

Figure 6. CNN architecture used in this study.

2.3.3. Utilized Optimizer

Deep learning utilizes abundant data and complex models for training; therefore, it consumes a lot of time for training. Particularly, the hyperspectral image used herein had 300 channels, compared to the general RGB image with 3 channels; thus, it took a long time for training. In addition to time, several hyperparameters need to be selected to reach the accuracy targeted by the algorithm. Changing the optimizer, which is a CNN hyperparameter, implies updating the weights in the training process to increase the training speed and performance. To identify the optimal algorithm suitable for the data to be used, training was performed using four optimizers and an appropriate model was selected.

- Stochastic Gradient Descent

Stochastic gradient descent (SGD), which is an algorithm that complements gradient descent (GD), is the most widely used optimizer for deep learning. It utilizes the gradient value and the learning rate to update the weights to minimize the value of the cost function, $J(\theta)$ in Equation (2). It is a form of moving after determining the direction and moving distance with respect to the current position of the weight value. Stochastic gradient descent does not use the entire training data but only uses a part of the data to perform the calculation.

$$\theta_{t+1} = \theta_t - \eta \nabla_\theta J(\theta) \tag{2}$$

It performs complementation through momentum because training proceeds very slowly when the gradient is very small [40]. Momentum is a way of providing inertia to the progress of SGD; i.e., remembering the way it moved before and making an additional move in that direction. Equation (3) expresses the movement vector that was used for the update after remembering the past movement.

$$v_t = \gamma v_{t-1} + \eta \nabla_{\theta_t} J(\theta_t) \tag{3}$$

- Adaptive Gradient

Adaptive gradient (AdaGrad) is an algorithm that changes the learning rate from the GD method to solve the following problem: if the learning rate is small, the training time is long, and if the learning rate is too large, it diverges [41]. In other words, if the process changes multiple times, the learning rate increases, and if the process change is small, the learning rate decreases to aid the training speed θ. In the process of updating θ, the learning rate was changed by dividing it by G_t, the gradient value used in the previous process in

Equation (4). When training progresses for a long time, the learning rate becomes so small that it barely moves and sometimes stops extremely early, which is disadvantageous.

$$G_t = G_{t-1} + \nabla_{\theta_t} J(\theta_t) \otimes \nabla_{\theta_t} J(\theta_t) \tag{4}$$

- Root Mean Square Propagation

Root Mean Square Propagation (RMSProp) is a method for solving the quick slow down and premature stoppage problems of AdaGrad [42]. Adaptive gradient simply utilizes all the gradient values in the past, whereas RMSProp uses the latest gradients while relatively maintaining them. Here, a new hyperparameter called attenuation rate (γ) was used, and it is included as an exponential average rather than a sum in Equation (5).

$$G_t = \gamma G_{t-1} + (1-\gamma) \nabla_{\theta_t} J(\theta_t) \otimes \nabla_{\theta_t} J(\theta_t) \tag{5}$$

- Adaptive Moment Estimation

Adaptive moment estimation (Adam) is an algorithm that combines momentum and RMSProp methods [42]. Similar to the momentum method, the value of the gradient so far is used, and it is stored as an exponential decaying average method. Then, using the RMSProp method, it is stored as an exponentially decreasing average of the squared gradients of the past. Further, since m and v are initialized to 0, a process is performed to prevent them from being biased to 0 at the beginning of training. Adam is the algorithm for updating the weights using the values that have undergone such a correction process, and the equation for θ update is as shown in Equation (6).

$$\theta_{t+1} = \theta_t - \frac{\eta}{\sqrt{\hat{v}_t + \epsilon}} \hat{m}_t \tag{6}$$

2.3.4. Performance Evaluation Index

The performance evaluation index used to create several models based on hyperparameters and compare the results is as follows. A confusion matrix refers to a table for comparing the actual and predicted values to measure the prediction performance through training. According to this table, the classification result is divided into four types: true positive (TP), false positive (FP), false negative (FN), and true negative (TN). Accuracy, which is a term often used in everyday life, refers to the proportion of parts that the model correctly classifies as described in Equation (7). Precision and recall are used to perform evaluations in terms of models and data, respectively, as shown in Equations (8) and (9). Finally, the F1 score shown in Equation (10) utilizes the harmonic mean value of precision and recall.

$$\text{Accuracy} = \frac{\text{TP} + \text{TN}}{\text{TP} + \text{FN} + \text{FP} + \text{TN}} \tag{7}$$

$$\text{Precision} = \frac{\text{TP}}{\text{TP} + \text{FP}} \tag{8}$$

$$\text{Recall} = \frac{\text{TP}}{\text{TP} + \text{FN}} \tag{9}$$

$$\text{F1 Score} = \frac{2 \times \text{Precision} \times \text{Recall}}{\text{Precision} + \text{Recall}} \tag{10}$$

3. Results and Discussion

3.1. Model Learning Time and Accuracy

To apply the CNN algorithm to hyperspectral images, several model hyperparameters were determined but some required tuning. Since this was a new type of data, no prior value existed. Thus, tuning was attempted through several iterations based on the existing values. Additionally, the size, number, and activation functions of the kernel of the convolutional layer mentioned in the CNN architecture were considered. The epoch at which training

was completed was identified through several random training processes, and the value that was sufficiently exceeded was determined as the overall epoch value. Based on this epoch value, early stopping was performed with patience of 300 using the validation loss to prevent overfitting. This served to terminate the training by ignoring the residual epoch if there was no improvement in the loss value during the subsequent 300 training sessions based on the loss value at a specific point in time. In the course of training, the best model of each optimizer was determined by noting the optimal model parameters through the validation loss value. Furthermore, each optimizer had its own hyperparameter, and it was modified according to the training and an appropriate value was used.

Table 2 presents the overall summary of the model creation and results for diagnosing the plant physiological disorders using the full-spectrum hyperspectral imaging data. The four optimizers used in the analysis were SGD with momentum, Adagrad, RMSProp, and Adam, and their characteristics were as follows. Among the four optimizers, Adam exhibited the best results. Although the overall training time was slower than that of RMSProp, it showed superior performance compared to other optimizers in classification accuracy. No significant difference was noted in terms of the speed for one epoch in the training process. RMSProp performed slightly similarly to Adam, and Adagrad was found to have poor performance and to take a very long time to train compared to the previous two optimizers. Especially, in most cases, SGD was not properly trained, and it was found that the performance of the SGD was not good because the classification results appeared randomly even after training.

Table 2. Optimization speed and plant physiological disorder classification accuracy for the optimizer.

Optimizer	Time (s)	Epochs	s/Epoch	Accuracy		
				Train	Validation	Test
SGD	6794.2	10,000	0.679	0.169	0.1761	0.145
Adagrad	1509.2	2246	0.672	0.935	0.918	0.933
RMSProp	513.4	753	0.682	0.951	0.957	0.957
Adam	724.7	1075	0.674	0.982	0.978	0.981

3.2. Analysis According to the Optimizers

3.2.1. Adagrad

Figure 7 depicts the graph of the training process for the Adagrad optimizer. In the graph, training loss, validation loss, training accuracy, and validation accuracy are examined for the epoch at the time. Compared to the other optimizers, the loss value gradually decreased and the accuracy increased without any exceptional values. Training proceeded with the default epoch set to 10,000, demonstrating progress beyond the 2000 epoch. Overall, the performance increase based on the number of learning processes proceeds relatively slowly. Presumably this phenomenon occurs because the learning rate is very low as the training progresses for a long time due to the characteristic of Adagrad to automatically update the learning rate. When looking at the results of the graph and other optimizers, it is interpreted that the improvement stopped as it no longer occurred due to the decrease in speed rather than premature termination due to overfitting. Furthermore, performance improvement can be expected if the early termination condition is relaxed or not used at all, but since the performance increase would not be greater than the time and cost involved, it was stopped as it was. Accordingly, Adagrad is usually used as an optimizer for simple problems, and the cause can be directly identified.

Figure 8 shows the test set evaluated using the model judged to be the best through Adagrad training, and the results are displayed as a confusion matrix. Since the classification performance for the test set was 93.33%, it can be seen that the classification was done properly to some extent. It showed perfect prediction for the NBd2 class. Wilt, NBd1, and KMpr classes showed relatively poor performance. Generally, if the training is insufficient, the performance of the class, which is relatively difficult to classify, is poor, or

the random distribution result can be checked for a large number of classes. In this case, it can be said that the former was the case. However, as shown in the performance graph, it was difficult to significantly improve the performance through additional training and changing hyperparameters.

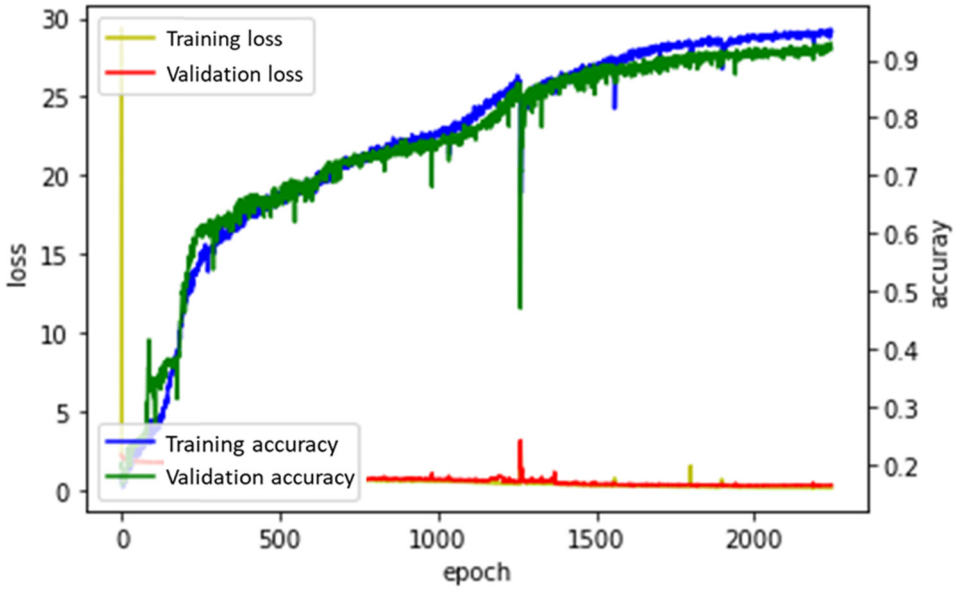

Figure 7. Performance graph by the Adagrad optimizer.

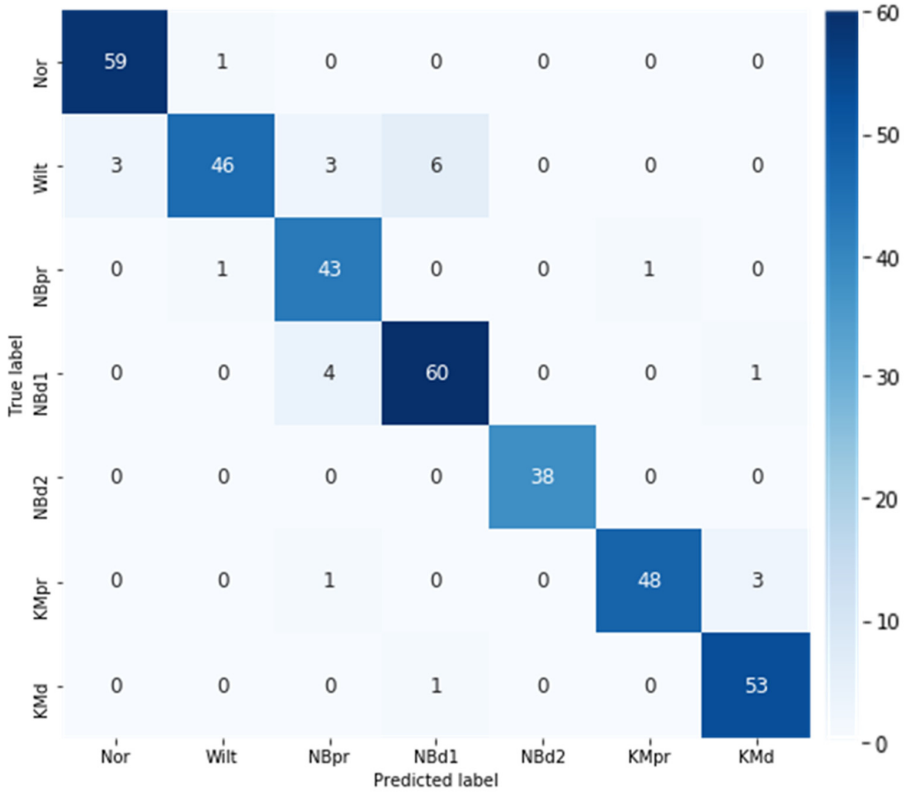

Figure 8. Test set confusion matrix for the Adagrad optimizer model.

3.2.2. RMSProp

Figure 9 shows the graph of the training process for the RMSProp optimizer. As the optimizer exhibiting the best classification performance after Adam, a relatively ideal and

stable graph was obtained in terms of classification accuracy. The training part, which rapidly increased at the beginning and slightly increased after a certain point, and the validation part, which displayed a similar shape to the training graph and decreased in the latter part, can be confirmed in the graph. In the loss graph, bouncing can be seen in many parts, which is interpreted as a case of jumping from a better local minima to a bad local minima during the training process. Although the adjustment of the learning rate value was necessary, no significant change in accuracy was noted; thus, it seemed to escape the bad local minima to some extent. If the epoch was $\geq$300, no significant performance improvement was noted. Therefore, if the early stopping part was a little tight, a significantly faster model with similar performance was afforded. It was determined that this fact can be advantageously used when training additional data to improve the model.

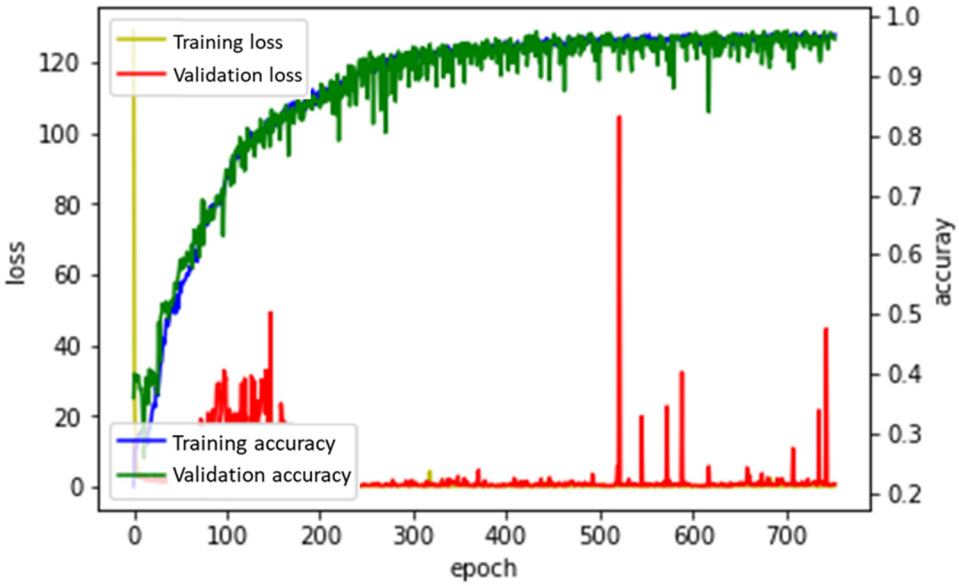

Figure 9. Performance graph by the RMSProp optimizer.

Figure 10 shows the test set evaluation results of the optimal model for the RMSProp optimizer. Since the classification performance was 95.70%, a confusion matrix with good results was yielded. Compared to the results of Adagrad, which had a relatively large misclassification in three classes, the number of classes was the same, but the overall prediction error was greatly improved. However, the NBpr class showed poor performance compared to the results of Adagrad. Overall, both the explanatory power of the data and the predictive explanatory power of the model were found to be good.

3.2.3. Adam

Figure 11 displays the graph of the training process for the Adam optimizer. Adam had a slower training speed than RMSProp, but was the optimizer that showed the best classification performance. The overall appearance of the graph is similar to that for the RMSProp, but it was confirmed that the splashing part of the loss was significantly reduced. Since Adam combines the ideas of the previous optimizers, the strengths and weaknesses of all optimizers were revealed together. In terms of model creation, the loss using the error calculation is a more important factor than accuracy. Additionally, in many cases, the time taken for training was not taken into consideration. Therefore, considering all aspects, it is judged that Adam was the most suitable optimizer.

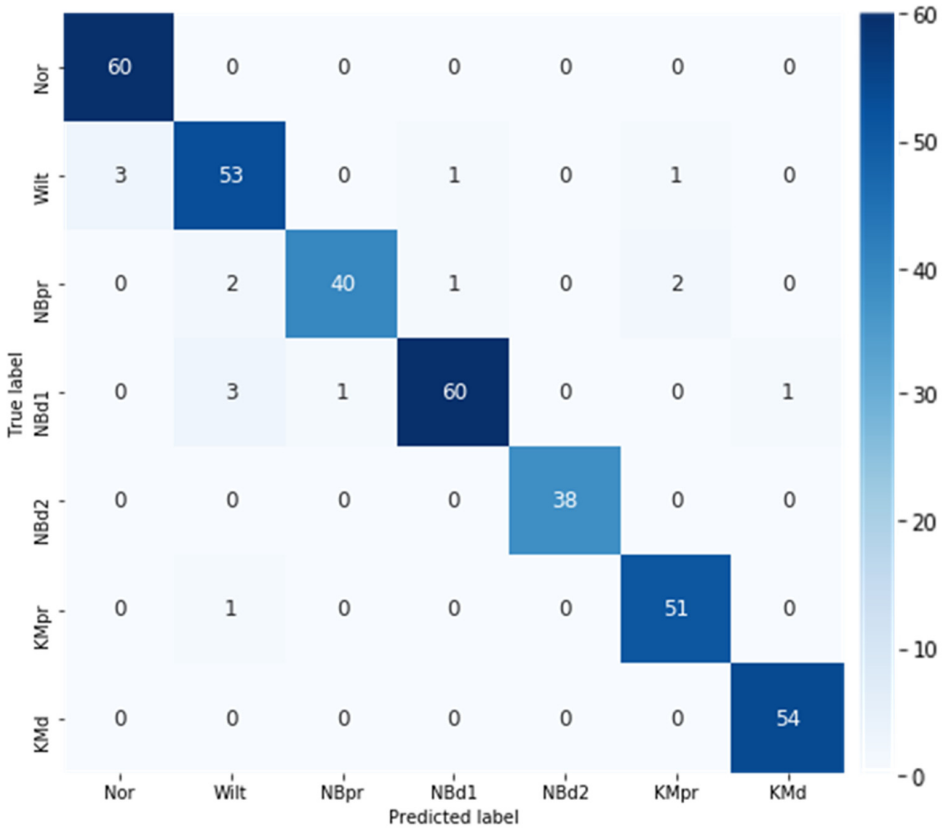

Figure 10. Test set confusion matrix for the RMSProp optimizer model.

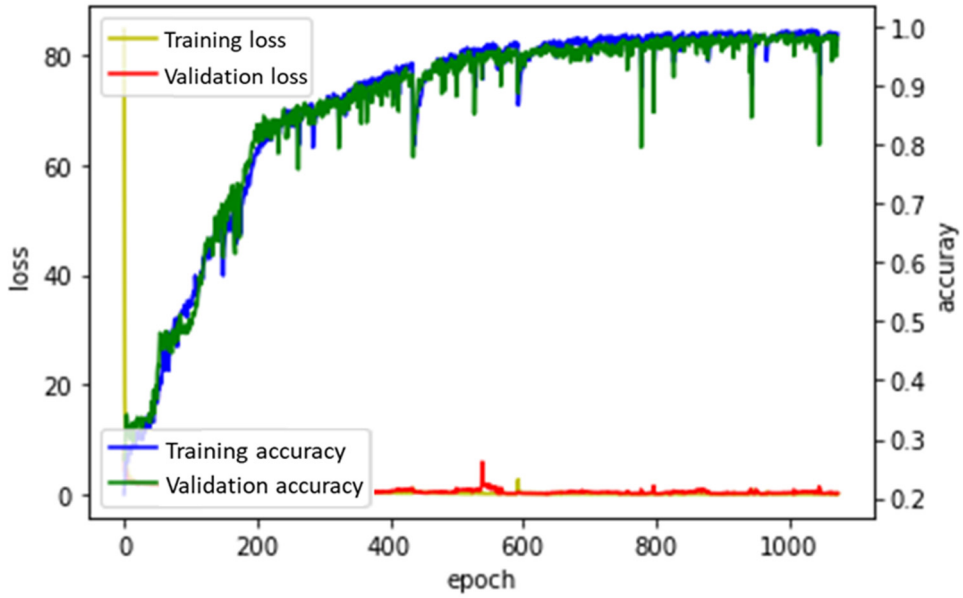

Figure 11. Performance graph by Adam optimizer.

Figure 12 shows the test set evaluation results of the optimal model for the Adam optimizer. Almost perfect classification was confirmed in all classes except for the wilt class. Three of the data of the wilt class were classified as normal class in all optimizers, and another two were found to show the same misclassification in Adam and RMSProp. In view of the classification form of this similar trend, it is judged that these misclassification data were difficult to classify by analysis using simple hyperspectral image cropping. Accordingly, it is expected that more accurate classification will be possible only when

additional feature information such as wavelength combination and texture identification is included.

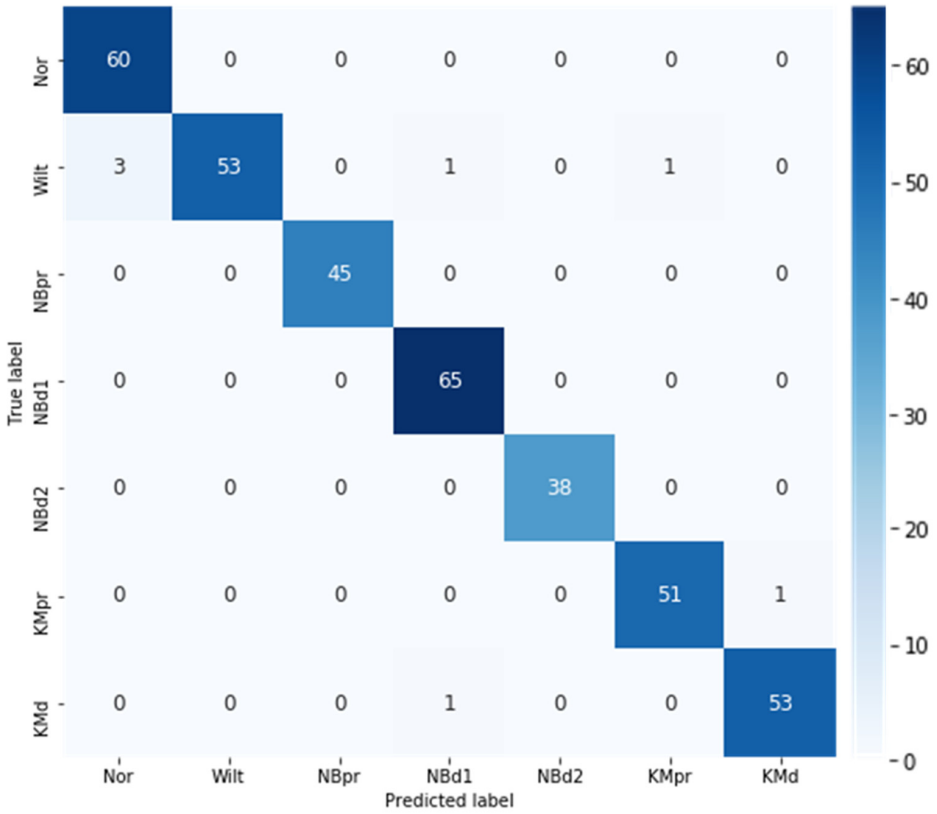

Figure 12. Test set confusion matrix for the Adam optimizer model.

3.3. Best Model Performance Evaluation

The Adam optimizer, which exhibited the best performance under the same conditions, was compared using a performance index (Table 3). Based on the weighted average, which is the average calculated by giving weights to the data of each class, it showed performance over 0.98. All classes except for the wilt class, which included data that were difficult to classify, afforded F1 scores of $\geq$0.98. As confirmed in the confusion matrix, both precision, which refers to the explanatory power of the model, and recall, which denotes explanation in terms of the true label data, showed similarly good performance. Although the RMSProp optimizer showed good performance, it was inferior to the Adam optimizer in all indices except learning speed.

Table 3. Performance evaluation index according to plant physiological disorders.

Class (Abbr.)	Precision	Recall	F1 Score
Normal (Nor)	0.95	1.00	0.98
Wilt (Wilt)	1.00	0.91	0.95
N, B deficiency prediction (NBpr)	1.00	1.00	1.00
N, B deficiency Stage 1 (NBd1)	0.97	1.00	0.98
N, B deficiency Stage 2 (NBd2)	1.00	1.00	1.00
K, Mg deficiency prediction (KMpr)	0.98	0.98	0.98
K, Mg deficiency (KMd)	0.98	0.98	0.98
Macro avg.	0.98	0.98	0.98
Weighted avg.	0.98	0.98	0.98

There have been several studies using hyperspectral images to detect and diagnose the onset of diseases in crop leaves [14,38,43]. However, when using various machine learning algorithms including deep learning, a small dataset was used or the existing spectral preprocessing method was used as it is. In this study, analysis using deep learning was performed on a sufficient amount of hyperspectral images without any special preprocessing on strawberry leaves, and the results showed similar performance to previous studies through the selection of optimal hyperparameters. In addition to the symptoms examined in this analysis, good performance can be expected if a large number of well-labeled training data can be secured. Although the result is good enough in terms of symptom prediction, it is judged that performance improvement is possible if additional non-destructive features other than spectral images, subimage size change, and transfer learning application are considered for more complete classification.

4. Conclusions

In this study, full-spectrum hyperspectral images were used to diagnose the physiological disorders in strawberry leaves. The model was created by applying the CNN algorithm without special spectroscopic preprocessing, and an optimal model was obtained through hyperparameter tuning and the performance evaluation of the optimizers. Adam, which afforded an F1 score of $\geq$0.95, was the best optimizer. In the case of RMSProp, the performance was slightly insufficient, but the applicability was identified in terms of training speed. During the diagnosis of physiological disorders, if environmental data, such as temperature, humidity, and soil moisture, and simple image analysis are additionally considered, more diverse analyses will be possible. Moreover, if a horticultural base is considered and applied to the hyperspectral image classification, the explanatory power of the model results could be increased. These results are expected to be applied to smart agriculture and utilized for high-throughput phenotypic analysis.

Funding: This work was supported by the National Research Foundation of Korea (NRF) grant funded by the Korea government (MSIT) (No. 2022R1C1C2005959).

Institutional Review Board Statement: Not applicable.

Informed Consent Statement: Not applicable.

Data Availability Statement: The data presented in this study are available on request from the corresponding author.

Acknowledgments: This research was supported by Smart Agriculture Innovation Center. This research was supported by Basic Science Research Program through the National Research Foundation of Korea (NRF) funded by the Ministry of Education (2016R1D1A1B03935534).

Conflicts of Interest: The author declares no conflict of interest.

References

1. Shah, D.; Tang, L.; Gai, J.; Putta-Venkata, R. Development of a mobile robotic phenotyping system for growth chamber-based studies of genotype x environment interactions. *IFAC-PapersOnLine* **2016**, *49*, 248–253. [CrossRef]
2. Kim, Y.; Glenn, D.M.; Park, J.; Ngugi, H.K.; Lehman, B.L. Hyperspectral image analysis for water stress detection of apple trees. *Comput. Electron. Agric.* **2011**, *77*, 155–160. [CrossRef]
3. Yang, M.; Cho, S.-I. High-Resolution 3D Crop Reconstruction and Automatic Analysis of Phenotyping Index Using Machine Learning. *Agriculture* **2021**, *11*, 1010. [CrossRef]
4. Ge, Y.; Atefi, A.; Zhang, H.; Miao, C.; Ramamurthy, R.K.; Sigmon, B.; Yang, J.; Schnable, J.C. High-throughput analysis of leaf physiological and chemical traits with VIS–NIR–SWIR spectroscopy: A case study with a maize diversity panel. *Plant Methods* **2019**, *15*, 1–12. [CrossRef] [PubMed]
5. Pandey, P.; Ge, Y.; Stoerger, V.; Schnable, J.C. High throughput in vivo analysis of plant leaf chemical properties using hyperspectral imaging. *Front. Plant Sci.* **2017**, *8*, 1348. [CrossRef] [PubMed]
6. Nguyen, H.T.; Lee, B.-W. Assessment of rice leaf growth and nitrogen status by hyperspectral canopy reflectance and partial least square regression. *Eur. J. Agron.* **2006**, *24*, 349–356. [CrossRef]
7. Elvanidi, A.; Katsoulas, N.; Ferentinos, K.; Bartzanas, T.; Kittas, C. Hyperspectral machine vision as a tool for water stress severity assessment in soilless tomato crop. *Biosyst. Eng.* **2018**, *165*, 25–35. [CrossRef]

8. Sabatier, D.R.; Moon, C.M.; Mhora, T.T.; Rutherford, R.S.; Laing, M.D. Near-infrared reflectance (NIR) spectroscopy as a high-throughput screening tool for pest and disease resistance in a sugarcane breeding programme. *Int. Sugar J.* **2014**, *116*, 580–583.
9. Li, F.; Mistele, B.; Hu, Y.; Chen, X.; Schmidhalter, U. Reflectance estimation of canopy nitrogen content in winter wheat using optimised hyperspectral spectral indices and partial least squares regression. *Eur. J. Agron.* **2014**, *52*, 198–209. [CrossRef]
10. Shen, L.; Gao, M.; Yan, J.; Li, Z.-L.; Leng, P.; Yang, Q.; Duan, S.-B. Hyperspectral estimation of soil organic matter content using different spectral preprocessing techniques and PLSR method. *Remote Sens.* **2020**, *12*, 1206. [CrossRef]
11. Zhou, X.; Sun, J.; Mao, H.; Wu, X.; Zhang, X.; Yang, N. Visualization research of moisture content in leaf lettuce leaves based on WT-PLSR and hyperspectral imaging technology. *J. Food Process Eng.* **2018**, *41*, e12647. [CrossRef]
12. Muangprathub, J.; Boonnam, N.; Kajornkasirat, S.; Lekbangpong, N.; Wanichsombat, A.; Nillaor, P. IoT and agriculture data analysis for smart farm. *Comput. Electron. Agric.* **2019**, *156*, 467–474. [CrossRef]
13. Wolfert, S.; Ge, L.; Verdouw, C.; Bogaardt, M.-J. Big data in smart farming—A review. *Agric. Syst.* **2017**, *153*, 69–80. [CrossRef]
14. Rumpf, T.; Mahlein, A.-K.; Steiner, U.; Oerke, E.-C.; Dehne, H.-W.; Plümer, L. Early detection and classification of plant diseases with support vector machines based on hyperspectral reflectance. *Comput. Electron. Agric.* **2010**, *74*, 91–99. [CrossRef]
15. Han, Q.; Li, Y.; Yu, L. Classification of glycyrrhiza seeds by near infrared hyperspectral imaging technology. In Proceedings of the 2019 International Conference on High Performance Big Data and Intelligent Systems (HPBD&IS), Shenzhen, China, 9–11 May 2019; pp. 141–145.
16. Gbodjo, Y.J.E.; Ienco, D.; Leroux, L. Toward spatio–spectral analysis of sentinel-2 time series data for land cover mapping. *IEEE Geosci. Remote Sens. Lett.* **2019**, *17*, 307–311. [CrossRef]
17. Masjedi, A.; Zhao, J.; Thompson, A.M.; Yang, K.-W.; Flatt, J.E.; Crawford, M.M.; Ebert, D.S.; Tuinstra, M.R.; Hammer, G.; Chapman, S. Sorghum biomass prediction using UAV-based remote sensing data and crop model simulation. In Proceedings of the IGARSS 2018—2018 IEEE International Geoscience and Remote Sensing Symposium, Valencia, Spain, 22–27 July 2018; pp. 7719–7722.
18. Roscher, R.; Waske, B.; Forstner, W. Incremental import vector machines for classifying hyperspectral data. *IEEE Trans. Geosci. Remote Sens.* **2012**, *50*, 3463–3473. [CrossRef]
19. Kamilaris, A.; Prenafeta-Boldú, F.X. Deep learning in agriculture: A survey. *Comput. Electron. Agric.* **2018**, *147*, 70–90. [CrossRef]
20. Krizhevsky, A.; Sutskever, I.; Hinton, G.E. Imagenet classification with deep convolutional neural networks. *Adv. Neural Inf. Processing Syst.* **2012**, *25*, 1–9. [CrossRef]
21. Han, Y.; Liu, Z.; Khoshelham, K.; Bai, S.H. Quality estimation of nuts using deep learning classification of hyperspectral imagery. *Comput. Electron. Agric.* **2021**, *180*, 105868. [CrossRef]
22. Yang, W.; Yang, C.; Hao, Z.; Xie, C.; Li, M. Diagnosis of plant cold damage based on hyperspectral imaging and convolutional neural network. *IEEE Access* **2019**, *7*, 118239–118248. [CrossRef]
23. Pérez-Pérez, B.D.; Garcia Vazquez, J.P.; Salomón-Torres, R. Evaluation of convolutional neural networks' hyperparameters with transfer learning to determine sorting of ripe medjool dates. *Agriculture* **2021**, *11*, 115. [CrossRef]
24. Saleem, M.H.; Potgieter, J.; Arif, K.M. Plant disease classification: A comparative evaluation of convolutional neural networks and deep learning optimizers. *Plants* **2020**, *9*, 1319. [CrossRef] [PubMed]
25. Labhsetwar, S.R.; Haridas, S.; Panmand, R.; Deshpande, R.; Kolte, P.A.; Pati, S. Performance Analysis of Optimizers for Plant Disease Classification with Convolutional Neural Networks. In Proceedings of the 2021 4th Biennial International Conference on Nascent Technologies in Engineering (ICNTE), Navi Mumbai, India, 15–16 January 2021; pp. 1–6.
26. Noon, S.K.; Amjad, M.; Qureshi, M.A.; Mannan, A. Overfitting mitigation analysis in deep learning models for plant leaf disease recognition. In Proceedings of the 2020 IEEE 23rd International Multitopic Conference (INMIC), Bahawalpur, Pakistan, 5–7 November 2020; pp. 1–5.
27. Selvam, L.; Kavitha, P. Classification of ladies finger plant leaf using deep learning. *J. Ambient. Intell. Humaniz. Comput.* **2020**, 1–9. [CrossRef]
28. Dyrmann, M.; Karstoft, H.; Midtiby, H.S. Plant species classification using deep convolutional neural network. *Biosyst. Eng.* **2016**, *151*, 72–80. [CrossRef]
29. Kussul, N.; Lavreniuk, M.; Skakun, S.; Shelestov, A. Deep learning classification of land cover and crop types using remote sensing data. *IEEE Geosci. Remote Sens. Lett.* **2017**, *14*, 778–782. [CrossRef]
30. Garnot, V.S.F.; Landrieu, L.; Giordano, S.; Chehata, N. Time-space tradeoff in deep learning models for crop classification on satellite multi-spectral image time series. In Proceedings of the IGARSS 2019—2019 IEEE International Geoscience and Remote Sensing Symposium, Yokohama, Japan, 28 July–2 August 2019; pp. 6247–6250.
31. Laban, N.; Abdellatif, B.; Ebeid, H.M.; Shedeed, H.A.; Tolba, M.F. Seasonal multi-temporal pixel based crop types and land cover classification for satellite images using convolutional neural networks. In Proceedings of the 2018 13th International Conference on Computer Engineering and Systems (ICCES), Cairo, Egypt, 18–19 December 2018; pp. 21–26.
32. Li, Z.; Chen, G.; Zhang, T. A CNN-transformer hybrid approach for crop classification using multitemporal multisensor images. *IEEE J. Sel. Top. Appl. Earth Obs. Remote Sens.* **2020**, *13*, 847–858. [CrossRef]
33. Zhang, N.; Yang, G.; Pan, Y.; Yang, X.; Chen, L.; Zhao, C. A review of advanced technologies and development for hyperspectral-based plant disease detection in the past three decades. *Remote Sens.* **2020**, *12*, 3188. [CrossRef]

34. Ariana, D.P.; Lu, R.; Guyer, D.E. Near-infrared hyperspectral reflectance imaging for detection of bruises on pickling cucumbers. *Comput. Electron. Agric.* **2006**, *53*, 60–70. [CrossRef]
35. Sarasketa, A.; González-Moro, M.B.; González-Murua, C.; Marino, D. Nitrogen source and external medium pH interaction differentially affects root and shoot metabolism in Arabidopsis. *Front. Plant Sci.* **2016**, *7*, 29. [CrossRef]
36. Nestby, R.; Lieten, F.; Pivot, D.; Lacroix, C.R.; Tagliavini, M. Influence of mineral nutrients on strawberry fruit quality and their accumulation in plant organs: A review. *Int. J. Fruit Sci.* **2005**, *5*, 139–156. [CrossRef]
37. Wang, J.; Liu, X.; Huang, F.; Tang, J.; Zhao, L. Salinity forecasting of saline soil based on ANN and hyperspectral remote sensing. *Trans. Chin. Soc. Agric. Eng.* **2009**, *25*, 161–166.
38. Grinblat, G.L.; Uzal, L.C.; Larese, M.G.; Granitto, P.M. Deep learning for plant identification using vein morphological patterns. *Comput. Electron. Agric.* **2016**, *127*, 418–424. [CrossRef]
39. Karpathy, A. Convolutional Neural Networks. Available online: http://cs231n.github.io/convolutional-networks (accessed on 18 September 2022).
40. Polyak, B.T. Some methods of speeding up the convergence of iteration methods. *USSR Comput. Math. Math. Phys.* **1964**, *4*, 1–17. [CrossRef]
41. Duchi, J.; Hazan, E.; Singer, Y. Adaptive subgradient methods for online learning and stochastic optimization. *J. Mach. Learn. Res.* **2011**, *12*, 2121–2159.
42. Ruder, S. An overview of gradient descent optimization algorithms. *arXiv* **2016**, arXiv:1609.04747.
43. Jiang, Q.; Wu, G.; Tian, C.; Li, N.; Yang, H.; Bai, Y.; Zhang, B. Hyperspectral imaging for early identification of strawberry leaves diseases with machine learning and spectral fingerprint features. *Infrared Phys. Technol.* **2021**, *118*, 103898. [CrossRef]